Front. Struct. Civ. Eng. 2022, 16(6): 685–703
https://doi.org/10.1007/s11709-022-0824-2

RESEARCH ARTICLE

Structural design and mechanical responses of closely spaced super-span double tunnels in strongly weathered tuff strata

Jiaxin HE, Shaohui HE*, Xiabing LIU, Jinlei ZHENG

School of Civil Engineering, Beijing Jiaotong University, Beijing 100044, China
**Corresponding author. E-mail: shhhe@bjtu.edu.cn*

ABSTRACT This paper presents a study of closely spaced double tunnels in Taizhou, China. One is Xiabei Mountain No. 2 four-line super-span high-speed railway tunnel (HRT), and the other is Xiabei Mountain double-line large-span subway tunnel (ST). The excavation spans of HRT and ST are 26.3 and 14 m, respectively. The two tunnels are located at different levels, and their separating distance is 17.2 m. Due to the short construction period, the HRT excavation was completed earlier than ST. The structural design of the HRT, taking account of the disturbance by the ST construction, was analyzed by a numerical simulation. It was found that the "yielding principle" design was more feasible than the "resistance principle" design when considering the safety and durability of the HRT secondary lining. The mechanical responses of the HRT during ST construction were comprehensively monitored and analyzed, including the vault settlement, horizontal convergence, surrounding rock pressure, and the internal stress in shotcrete and steel arch. Results show that the longitudinal influence range of the ST construction on the HRT was approximately 0.6–1.1 times the ST outer diameter; the disturbance was mainly generated in the ST upper bench excavation; and the final axial force of the HRT shotcrete was approximately 9–16 times that of the steel arch, which indicated that the shotcrete was the main bearing structure. The safety status of the HRT was assessed based on the monitoring data, and the minimum safety factors of the HRT shotcrete and steel arch were 1.61 and 1.89, respectively. Parametric studies were performed to show how the lining stress of HRT was affected by the relative angle, pillar width, ST excavation method and excavation footage. Finally, the design and construction optimization were proposed according to the monitoring data and parameter analysis results. This study might provide practical reference for similar projects.

KEYWORDS double tunnels, super-span, structural design, mechanical response, numerical simulation, field monitoring

1 Introduction

Closely spaced double tunnels are divided into leading and lagging tunnels according to the construction sequence. Generally, to reduce the construction risk, the lagging tunnel is not excavated until a certain length of the leading tunnel has been constructed [1,2]. However, lagging tunneling may threaten the leading tunnel due to their narrow rock pillar [3,4]. On the one hand, the lining behaviors of the leading tunnel are closely related to its structural design. Therefore, selecting a robust design is key to the safety of the leading tunnel [5]. On the other hand, there are multiple changes in the surrounding rock pressure and lining stress of the leading tunnel under the lagging tunnelling. Thus, investigating the mechanical response during lagging tunnelling is significant to the construction safety and design optimization [1,2].

Numerical simulations [6–9], theoretical analysis [10–12], laboratory modelling [13,14], and field monitoring [15–17] have been used to study the mechanical behaviors of closely spaced tunnels. These studies have promoted the understanding of the mechanical response of closely spaced double tunnels and provided an essential reference for the design optimization of the support. However, the existing studies mainly focus on the mechanical behaviors of closely spaced double

Article history: Received Sep 26, 2021; Accepted Jan 11, 2022

tunnels without separately considering the construction influence of the lagging tunnel on the leading tunnel and its ongoing construction. Generally, the considerable disturbance induced by lagging tunnelling may lead to lining failure in the leading tunnel [1]. However, few studies have systematically analyzed the excavation disturbance of lagging tunnels. Wu et al. [3] and Do et al. [4] investigated the disturbance caused by lagging tunnelling considering the effects of the lagged distance, pillar width, and relative tunnel orientation by numerical simulation. Based on field monitoring, Li et al. [1] studied the surrounding rock pressure, circumferential stress in shotcrete and axial stress in the steel frame of closely spaced large-span triple tunnels. It can be concluded that with the decrease in pillar width, the excavation influence of the middle tunnel on the side tunnels became significant. Huang et al. [18] used a numerical method to investigate the mechanical response of an existing shield tunnel during construction of a lagging shield tunnel. The results showed that the maximum ground settlement of the leading tunnel occurred at the arch waist, and the maximum lining stress increased by 44% during the construction of the lagging shield tunnel. However, the tunnel spans in the above studies were all less than 16 m. Compared with traditional large-span tunnels, super-span tunnels with spans greater than 25 m have more complex structures. Their complex excavation procedure leads to multiple changes in the surrounding rock pressure and lining stress. Thus, there are higher risks in closely spaced super-span double tunneling, which served as this paper's study background.

One such tunnel is the Hang-Shao-Tai high-speed railway Xiabei Mountain No. 2 super-span tunnel (HRT), and the other is the Taizhou subway Line S1 Xiabei Mountain large-span tunnel (ST). The rock mass in the project was mainly weathered tuff with a strong weathering zone in the local area. The two tunnels were located at different levels, and the spans of HRT and ST were 26.3 and 14 m, respectively. The structural design of HRT considering the construction influence of ST was analyzed by numerical simulation. The mechanical response of HRT during the excavation of ST was comprehensively investigated by field monitoring. The safety condition of HRT was assessed based on the measured values and some engineering suggestions were proposed. The results of this study can provide specific references for the design and construction of closely spaced super-span double tunnels.

2 Project overview

2.1 Tunnel situation and geological condition

The HRT is the key component of the Hang-Shao-Tai high-speed railway, and is designed to be a four-line super-span tunnel due to its proximity to the Taizhou Railway Station (approximately 795 m apart). The maximum cover depth is 57.4 m, the total length is 430 m (from DK215+055 to DK215+485), and the excavation span and area are 26.3 m and 361 m^2, respectively. The ST is an important link connecting the Taizhou Railway Station and Development Avenue Station of Taizhou Metro Line S1. ST was designed to be a double-line tunnel, the cover depth varies from 25 to 76.3 m, and the excavation span and area are 14 m and 135.8 m^2, respectively. As shown in Fig. 1, the two tunnels are roughly parallel in the longitudinal direction but not on the same level in the vertical direction. The horizontal net distance between the two tunnels is approximately 12.7 m. The vertical height difference of the tunnel inverts is approximately 14.4 m. The tunnel relative positions on the longitudinal section and cross-section are displayed in Figs. 2 and 3, respectively.

As displayed in Fig. 2, the rock mass is mainly composed of tuff and silty clay. The silty clay layer covers the mountain surface with a thickness of 2 m. The tuff stratum near the tunnel entrance (form DK215+055 to DK215+121) was classified as Class V according to the BQ rock mass classification system (China), and the tuff stratum at the tunnel body was classified as Class III or IV. The simplified relationship between the Chinese classification BQ system and the widely used Q system is shown in Table 1 [19]. As shown in Fig. 4, the very poor rock mass (Class-V ground) in the tunnel entrance is strongly weathered tuff, the rock block diameter is distributed in the range of 2–30 cm, and a clay layer with a thickness of approximately 1–5 cm is developed in the local area of joint fracture. Overall, the rock mass is relatively soft with a loose structure and poor cohesiveness, but groundwater is not present.

2.2 Excavation and support parameters

Compared with a fair rock mass (Class-III ground) or poor rock mass (Class-IV ground), a very poor rock mass (Class-V ground) leads to a more considerable load effect on the supporting system since the HRT span is extremely large. Therefore, the closely spaced tunneling of HRT and ST in very poor rock masses has a high risk during construction; the structure design method and the mechanical response of closely spaced super-span double

Fig. 1 Construction site of HRT and ST

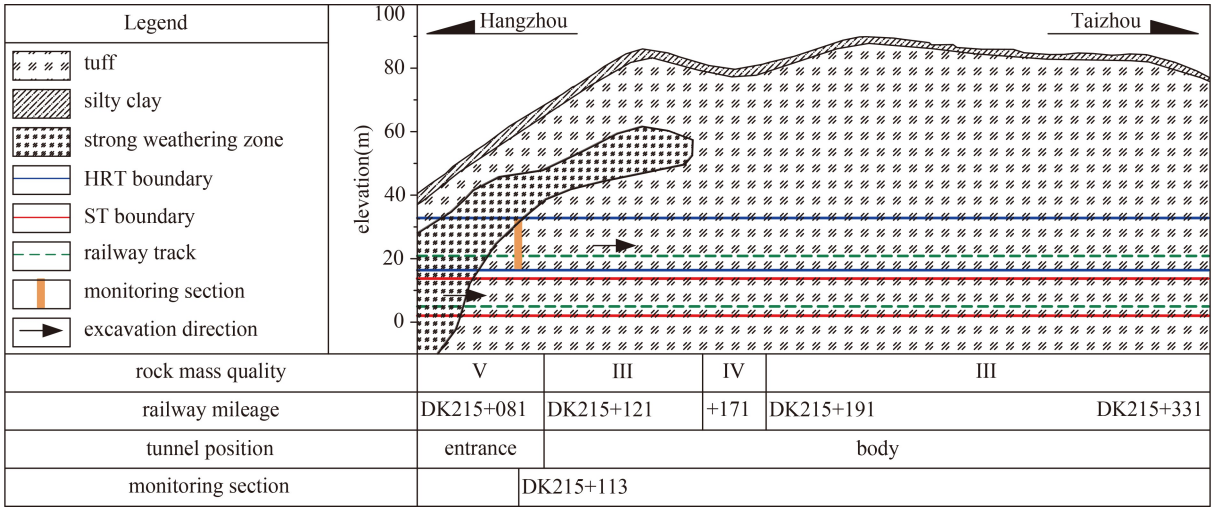

Fig. 2 Tunnel longitudinal section and geological conditions.

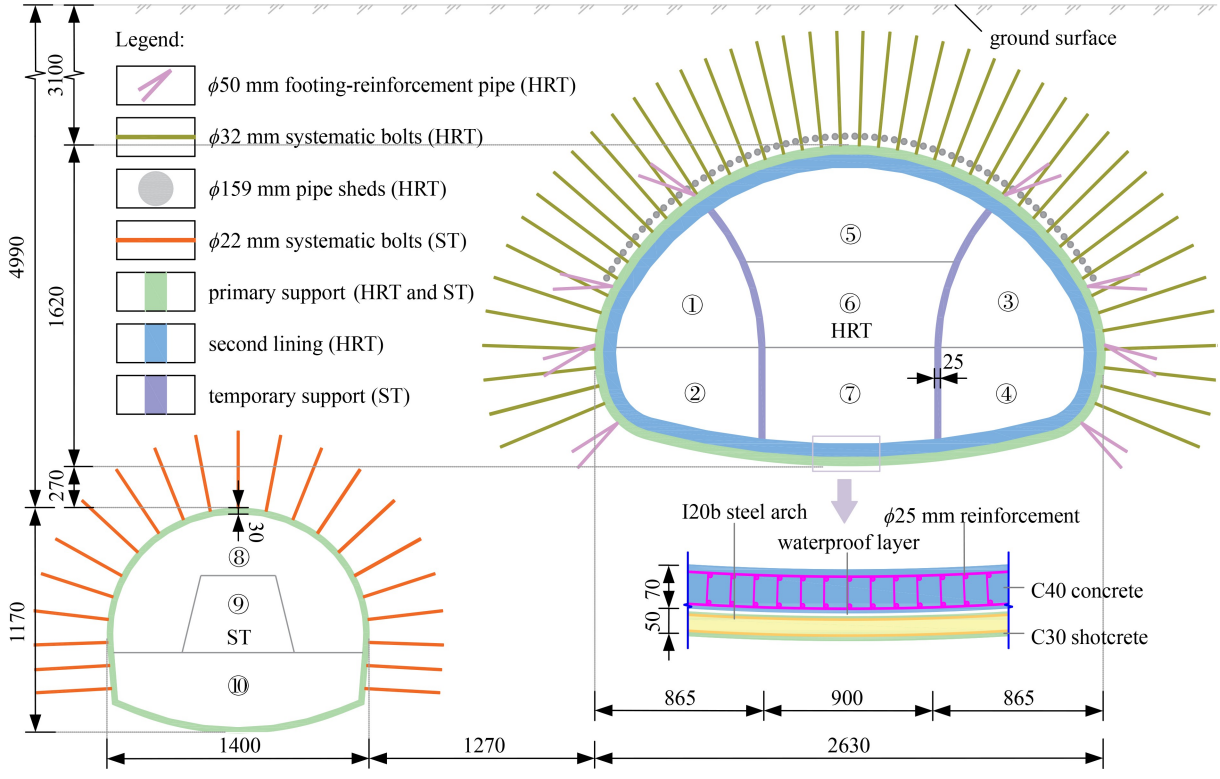

Fig. 3 Tunnel cross-section and support system in DK215+113 (unit: cm).

Table 1 Relationship between BQ system and Q system

type	Class I (very good)	Class II (good)	Class III (fair)	Class IV (poor)	Class V (very poor)
BQ system	> 550	451–550	351–450	251–350	< 250
Q system	> 40	10–40	4–10	1–4	< 1

tunnels in tunnel entrances were selected as the research targets.

The double side heading method was adopted for HRT based on the excavation size, geological conditions, and support form. This construction method has high construction efficiency since it can simplify the construction process and facilitate the use of large machinery. As shown in Fig. 3, the HRT was divided into 7 headings for drilling and blasting. The excavation sequence was ①→②→③→④→⑤→⑥→⑦. The excavation footage of each heading was 0.8 m, and the lagging distance was 15–20 m. All the headings were excavated using the bench cut method, and the bench length was 10 m for the side headings and 15 m for the

middle headings. The ST construction methods depended on the surrounding rock condition: full-section construction method for Class-III ground and bench cut method for Class-IV or Class-V ground. The ST excavation footage was 1.2 m, and the bench length was 10 m. For the tunnel entrance, the ST was divided into 3 headings and the excavation sequence was ⑧→⑨→⑩.

As shown in Fig. 3, composite support, including primary support (steel arch, shotcrete, and systematic bolts), temporary support (steel arch and shotcrete), water-proof layer, and secondary lining (reinforcement and cast-in-place concrete), was adopted in this project. At the tunnel entrance, auxiliary methods such as pipe roofs and footing-reinforcement pipes were applied to ensure the HRT safety and stability. The supporting parameters in the tunnel entrance are listed in Table 2.

3 Comparison of high-speed railway tunnel structural designs

3.1 High-speed railway tunnel structural designs

In the preliminary design, the ST is desirable to be excavated first to avoid its adverse effect on the HRT construction. However, due to the short construction period of the Hang-Shao-Tai high-speed railway and the small distance between the HRT and Jiaojiang Bridge (Fig. 1), the HRT is constructed before the ST so as to provide construction conditions for Jiaojiang Bridge. This ST construction can inevitably cause considerable disturbance to the HRT, which may cause significant construction risk for the HRT construction. Generally, two structural designs can be used for the HRT taking account of the ST construction disturbance: the "yielding principle" design and the "resistance principle" design [20]. For the "yielding principle" design, the primary support deformation in the HRT is allowed to release the surrounding rock pressure induced by the ST construction, and the secondary lining of the HRT is not applied until the primary support and surrounding rock reach equilibrium. For the "resistance principle" design, the secondary lining is implemented as soon as possible. The disturbance caused by the ST construction is resisted by the strong support system composed of a primary support and a secondary lining. Accordingly, the construction sequences of the two structural designs are as follows:

1) "Yielding principle" design: HRT excavation and primary support construction → ST excavation and primary support construction → HRT secondary lining construction;

2) "Resistance principle" design: HRT excavation and primary support construction → HRT secondary lining construction → ST construction and primary support

Fig. 4 Excavation exposure of tunnel entrance (Class-V ground).

Table 2 Tunnel supporting parameters in Class-V ground

supports	structures	parameters	installation area
auxiliary methods (HRT)	pipe roof	ϕ159 mm steel pipes; L = 60 m	tunnel portal
	footing-reinforcement pipes	ϕ50 mm seamless steel pipes; L = 6 m; t = 4 mm	tunnel arch and side wall
primary support (HRT)	shotcrete	thickness: 50 cm type: steel fiber reinforced shotcrete, C30	whole section
	steel arch	I20b; longitudinal spacing: 0.8 m	whole section
	systematic bolts	ϕ32 mm hollow grouted bolts; L = 6 m longitudinal and circumferential spacing: 1.0 m × 0.75 m	side wall and arch
temporary support (HRT)	shotcrete	thickness: 25 cm type: steel fiber reinforced shotcrete, C30	whole section
	steel arch	I20b; longitudinal spacing: 0.8 m	whole section
secondary lining (HRT)	cast-in-place concrete	thickness: 70 cm; type: C40	whole section
	reinforcement	ϕ25 mm main reinforcements longitudinal and circumferential spacing: 0.2 m × 0.2 m	whole section
primary support (ST)	shotcrete	thickness: 30 cm; type: C30	whole section
	steel arch	I18; longitudinal spacing: 0.6 m	whole section
	systematic bolts	ϕ22 mm hollow grouting bolts spacing in the side wall: 1.5 m × 1.5 m spacing in the arch: 1.2 m × 1.0 m	side wall and arch

construction.

A three-dimensional numerical simulation of the construction process is performed using a finite difference program. By comparing the simulated stress state of the tunnel lining, the displacement and plastic zone of the surrounding rock, a more feasible structural design for the HRT is determined.

3.2 Numerical model

The tunnel entrance with mileage markers of DK215+055–DK215+121 was analyzed to ensure that the numerical simulation truly reflected the field situation. Based on the FLAC3D program, a computational model including the topography of Xiabei Mountain was established (Fig. 5). According to the modified Fenner formula in an ideal elastic-plastic rock mass [21], the stress field of the surrounding rock outside 4 times the excavation radius remained unchanged. Therefore, the model span was set to be approximately 9 times the HRT span, and the distance from the model bottom to the HRT invert was set to be 4 times the HRT height. Consequently, the model's transverse width, longitudinal length and vertical height were 240, 66, and 130 m, respectively. Normal constraints were set on the four sides of the model, and fixed constraints were set on the model bottom.

The surrounding rock and the tunnel lining were assumed to be homogeneous media and were simulated by hexahedral solid elements. The Mohr−Coulomb criterion was adopted for the surrounding rock mass, and a linear elastic model was adopted for the tunnel linings. The influence of groundwater was not considered since groundwater was not present. For silty clay, the calculation parameters were determined based on previous numerical simulation experience [5,22]. For Class-V tuff strata, laboratory tests were carried out on the tuff samples drilled from the field, and the strength parameters, uniaxial compressive strength and elastic modulus of the rock blocks were 10.8 MPa, 25.8 MPa and 15.14 GPa, respectively. According to the site geological conditions and the GSI value determination method [23], the GSI value of Class-V tuff strata was determined to be 12, and the disturbance coefficient was 0.7. The calculation parameters of Class-V tuff strata were calculated based on the Hoek-Brown strength criterion [24]. The steel arch was converted into concrete according to its elastic modulus to simplify the numerical model, and the calculation formula is shown in Eq. (1) [25]. The calculation parameters of the surrounding rock and the tunnel linings are listed in Table 3.

$$E = E_c + E_s \frac{S_s}{S_c}, \tag{1}$$

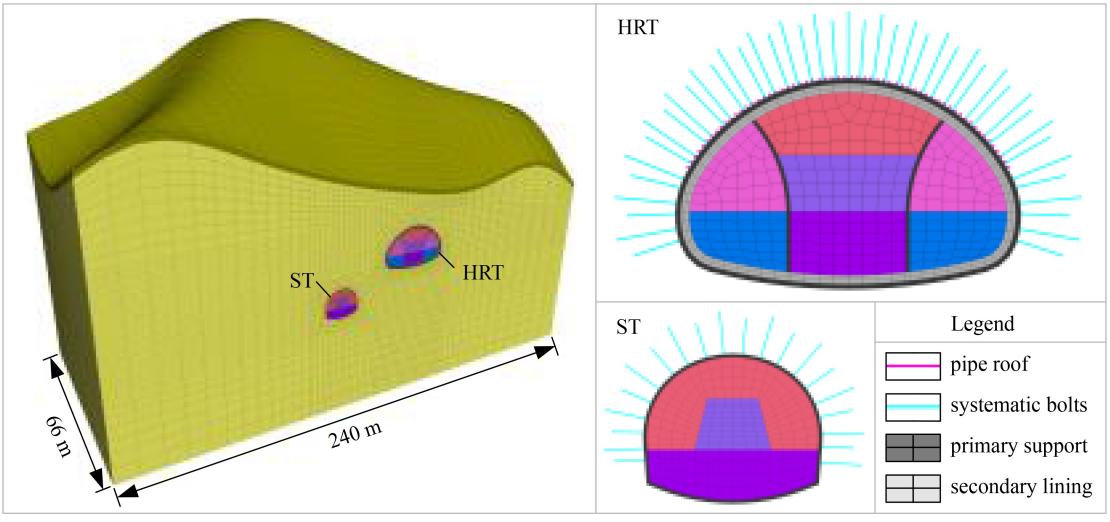

Fig. 5 Numerical model.

Table 3 Calculation parameters of surrounding rock and tunnel lining

strata and lining	thickness (m)	gravity density (kN·m^{-3})	elastic modulus (GPa)	Poisson's ratio	cohesion (kPa)	internal friction angle (°)
silty clay	2	19.5	0.07	0.36	31	28.5
tuff strata (Class-V)	80–128	22	0.35	0.33	254	9.1
primary support (HRT)	0.5	25	26.6	0.2	–	–
temporary support (HRT)	0.25	25	28.2	0.2	–	–
secondary lining (HRT)	0.7	25	34.9	0.2	–	–
primary support (ST)	0.3	25	27.0	0.2	–	–

where E_c and E are the elastic moduli of concrete before and after modification, respectively; E_s is the elastic modulus of the steel arch; and S_c and S_s are the cross-sectional areas of the concrete and steel arch, respectively. According to the Code for Design of Railway Tunnel (TB10003-2016) [26], the elastic moduli of C30 shotcrete, C40 cast-in-place concrete and I20b steel arch are 25, 33.5, and 200 GPa, respectively.

The systematic bolts were simulated by the cable units. The coupling-springs between the cable element nodes and solid element nodes in FLAC 3D program were used to simulate the interaction between the system bolts and surrounding rock; the stiffness of the coupling-springs was negatively correlated with the nodes spacing. The calculation parameters of the systematic bolts were determined by the simulated bolt pull-out test. The pipe roof was simulated by beam units. Similarly, the interaction between the pipe roof and surrounding rock was simulated by the coupling-springs between the beam unit nodes and solid element nodes. The simulation parameters of the pipe roof were calculated based on its geometrical dimension. The calculation parameters of the systematic bolts and pipe roof are listed in Tables 4 and 5.

The excavation sequence of HRT in simulation was ①→②→③→④→⑤→⑥→⑦, and the excavation footage of each heading was 0.8 m. The ST was excavated using the bench cut method. The excavation footage was 1.2 m, and the bench length was 10 m. Overall, the excavation method and supporting parameters of HRT and ST in the simulation were consistent with those in the field construction.

3.3 Simulation results

The simulation results of DK215+113 were analyzed since it was near the strong weathering zone in the field construction. The cover depths of HRT and ST at this cross-section were 31 and 49.9 m, respectively. The numerical results, including the lining stress, surrounding rock displacement and plastic zone, were analyzed and compared to determine the practical structural design.

3.3.1 Internal force of the tunnel lining

The lining stress in the simulation had a linear distribution since the linearly elastic model was adopted. Thus, the circumferential stress σ and bending moment M of the tunnel lining could be calculated by Eq. (2) [1].

$$\begin{cases} \sigma = \dfrac{1}{2}(\sigma_{in} + \sigma_{out}), \\ M = \dfrac{1}{2}(\sigma_{in} - \sigma_{out})W, \end{cases} \tag{2}$$

where σ_{in} and σ_{out} denote the circumferential stress on the inner and outer flanges of the tunnel lining, respectively; W represents the bending modulus and can be calculated by $W = bh^2/6$; b is the longitudinal length of the lining and is taken as 1 m here; and h is the lining thickness.

The safety factor is a critical parameter for the quantitative evaluation of lining safety. According to the Code for Design of Railway Tunnel (TB10003-2016) [26], the lining bearing capacity is controlled by the compressive strength when the eccentricity e_0 is less than or equal to 0.2 h. Otherwise, the bearing capacity is dominated by the tensile strength. The lining safety Factor K can be calculated by Eq. (3):

$$\begin{cases} K \leqslant \varphi\alpha R_c/\sigma, & e_0 \leqslant 0.2h, \\ K \leqslant \varphi \dfrac{1.75R_t}{\sigma(6e_0/h - 1)}, & e_0 > 0.2h, \end{cases} \tag{3}$$

where R_c and R_t denote the ultimate compressive strength and ultimate tensile strength of concrete, respectively; the eccentricity e_0 can be calculated by $e_0 = M/\sigma bh$; φ is the buckling coefficient and is equal to 1 for a tunnel project; and α denotes the acentric factor and can be calculated by $\alpha = 1 - 1.5e_0/h$.

The circumferential stress distributions and the safety factors of the HRT lining in the two structural designs are shown in Fig. 6 and Table 6, respectively. Because the lining internal force changed with the construction process, the circumferential stresses plotted in Fig. 6 were the maximum values, and the safety factors listed in Table 6 were the minimum values. It is specified that the stresses were positive in compression and negative in tension.

The circumferential stress distributions of the HRT lining in the two different structural designs were

Table 4 Calculation parameters of systematic bolts

bolts position	area (m^2)	elastic modulus (GPa)	grout-stiffness ($kN \cdot m^{-2}$)	grout-cohesion (MPa)	grout-friction (°)	grout-perimeter (m)	yield-tension (kN)
anchor head	3.52×10^{-4}	200	1.12×10^6	17.5	50	0.314	140
anchorage section	3.52×10^{-4}	200	1.12×10^4	0.175	30	0.314	140

Table 5 Calculation parameters of pipe roof

type	area (m^2)	gravity density ($kN \cdot m^{-3}$)	elastic modulus (GPa)	inertia moment-z (m^4)	inertia moment-x (m^4)	Poisson's ratio
pipe roof	4.68×10^{-3}	78.5	200	1.3×10^{-5}	1.3×10^{-5}	0.27

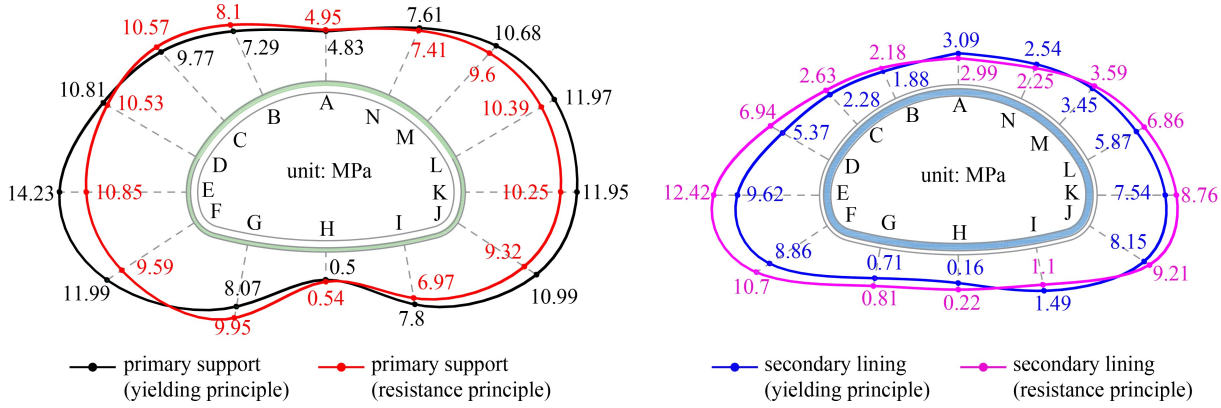

Fig. 6 Circumferential stress distribution of HRT linings in different structural designs.

Table 6 The safety factors of HRT lining in different structural designs

designs	support types	minimum safety factor (compressive strength control)		minimum safety factor (tensile strength control)	
		values	positions	values	positions
yielding principle	primary support	1.55	left wall waist (E)	1.62	left arch shoulder (B)
	secondary lining	3.84	left wall waist (E)	4.23	crown (A)
resistance principle	primary support	2.03	left wall waist (E)	2.34	middle invert (H)
	secondary lining	2.97	left wall waist (E)	1.53	left invert (G)

relatively similar. The circumferential stress on the left side of the HRT was greater than that on the right side. The maximum circumferential stress of the HRT primary support in the "yielding principle" design was 14.23 MPa, which was larger than 10.85 MPa in the "resistance principle" design. This finding indicates that the "resistance principle" design is better when considering the safety of the HRT primary support. However, the maximum circumferential stress of the HRT secondary lining in the "yielding principle" design was 9.62 MPa, which was smaller than the 12.42 MPa in the "resistance principle" design. This result indicates that the "yielding principle" design is more reliable given the secondary lining safety. Therefore, a quantitative analysis of HRT lining safety is required.

The safety factors in Table 6 were greater than the minimum safety factor of 1.5 specified in the Code for Design of Railway Tunnel (TB10003-2016) [26], indicating that the two structural designs were both feasible. For HRT primary support, the minimum safety factor in the "yielding principle" design was 1.55, slightly less than the 2.03 in the "resistance principle" design. However, the minimum safety factor of the HRT secondary lining in the "resistance principle" design was 1.53, which was significantly smaller than the value of 3.84 in the "yielding principle" design. This can be attributed to the ST construction disturbance on the HRT secondary lining in "resistance principle" design. The secondary lining of an HRT was always affected by concrete carbonation, train vibration and other durability factors during operation. The secondary lining of HRT needed a higher safety reserve to ensure the HRT safety and durability. Therefore, the "yielding principle" design was more feasible than the "resistance principle" design.

3.3.2 Vertical displacement and plastic zone of the surrounding rock

The vertical displacement and plastic zone area were crucial indices in evaluating the safety and stability of the surrounding rock. The final isoline map of the vertical displacement of the two different structural designs is shown in Fig. 7. The vertical displacement distributions of the two structural designs were relatively similar. The vault subsidence of HRT was much greater than that of the ST. One reason was the HRT enormous span and complex construction procedures, and the other was the secondary disturbance caused by the ST construction. The maximum settlement and uplift of the surrounding rock occurred at the vault and invert of the HRT, respectively. The vault subsidence of HRT in the "yielding principle" design and the "resistance principle" design were 80.9 and 72.5 mm, respectively, and the difference between the two structural designs was only 8.4 mm. As displayed in Fig. 8, the plastic zone distributions of the two structural designs were almost the same. The plastic zone near the HRT was mainly generated in the HRT arch shoulder, arch foot and wall foot.

Based on the above analysis, conclusions can be made that the two structural designs are both feasible given the safety of the HRT lining, and that there is little difference between these two designs in the surrounding rock

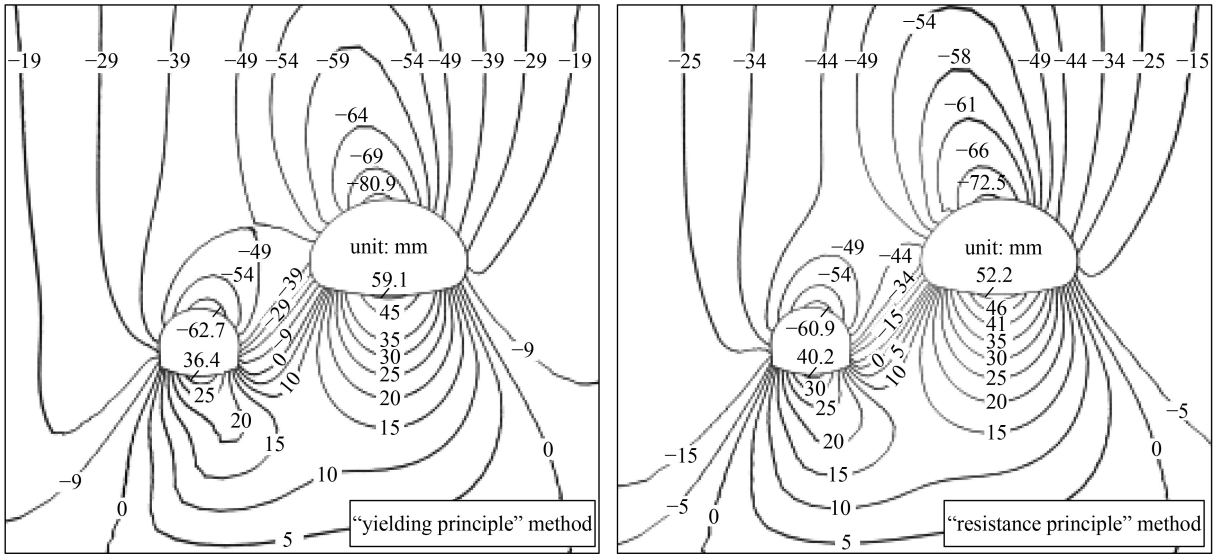

Fig. 7 Isoline map of vertical displacement in different structural designs.

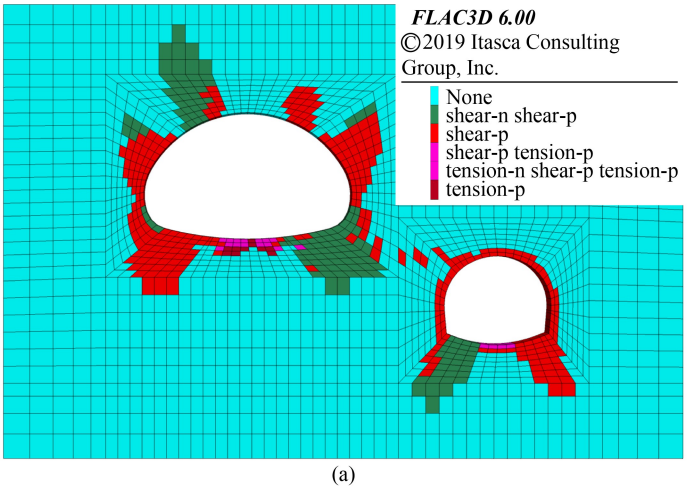

(a)

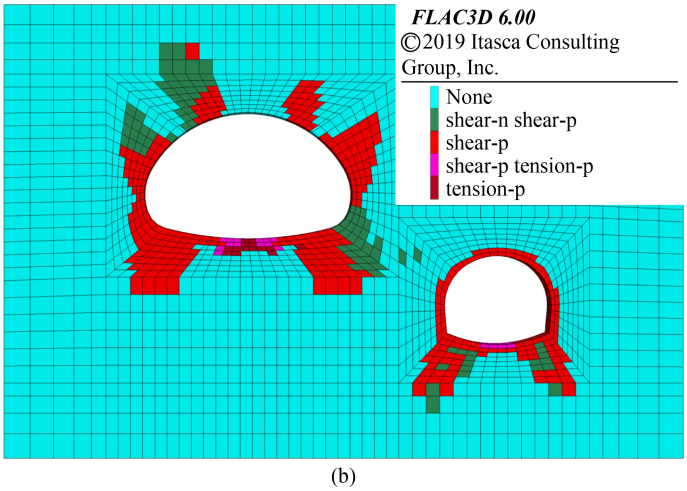

(b)

Fig. 8 Plastic zone distribution in different structural designs. (a) “Yielding principle” design; (b) “resistance principle” design.

vertical displacement and plastic zone. However, the minimum safety factor of the HRT secondary lining in the “yielding principle” design is approximately 2 times that in the “resistance principle” design. Therefore, the

"yielding principle" design is more feasible because the secondary lining of HRT needs a higher safety factor to resist durability degradation.

4 Field monitoring

4.1 Monitoring scheme

The "yielding principle" design was adopted in the field construction. The representative cross-section of DK215+113 (Class-V ground) was selected for field monitoring to investigate the implementation effect of this design and verify its reliability. The monitoring points on DK215+113 were arranged as shown in Fig. 9. A total of 14 monitoring points were arranged, with 7 measuring points located in the arch, 4 located on the sidewall and 3 located in the invert. As shown in Fig. 10, double-membrane pressure cells were installed against the surrounding rock with a steel bar fixed on the steel arch to measure the surrounding rock pressure. Concrete strain gauges were embedded in the shotcrete to measure the circumferential stress of the shotcrete. Steel surface strain gauges were welded on the inner and outer flanges of the steel arch to measure the axial stress. Total stations were used to measure the settlement and horizontal

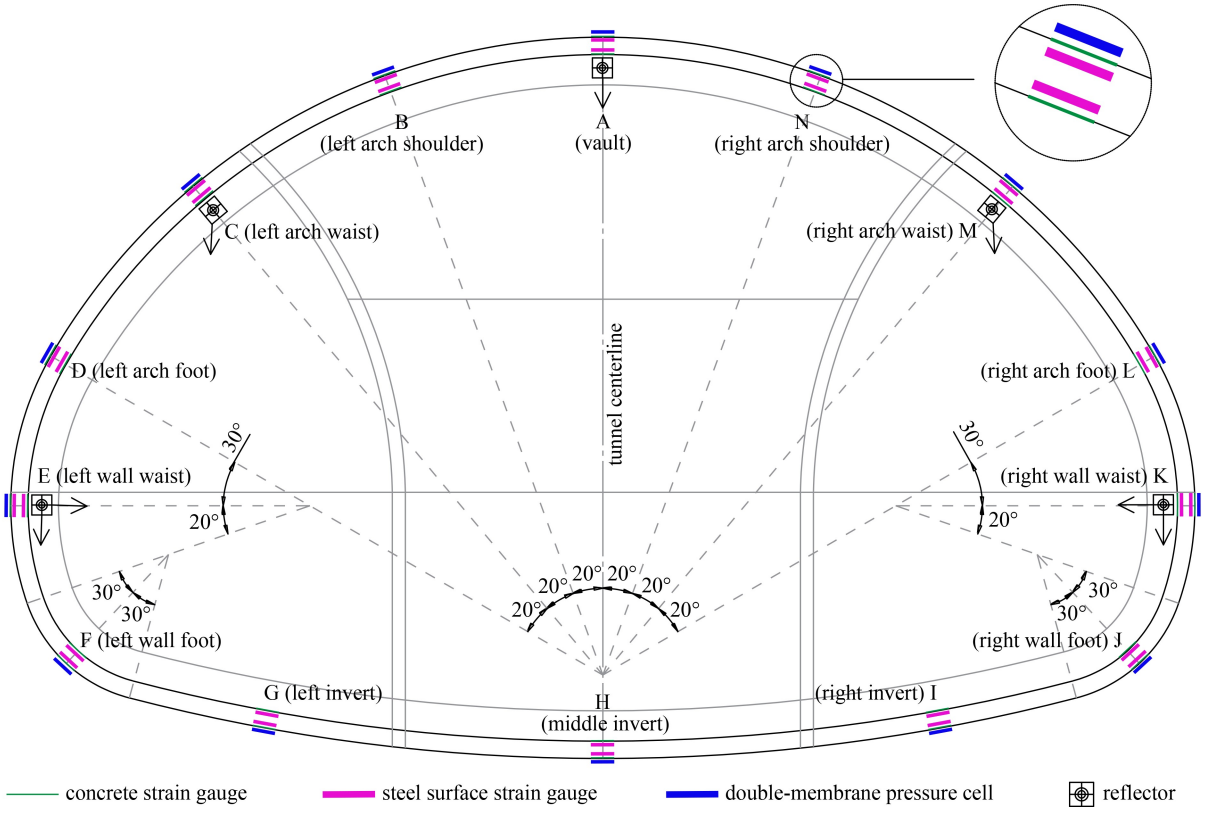

Fig. 9 Monitoring points arrangement.

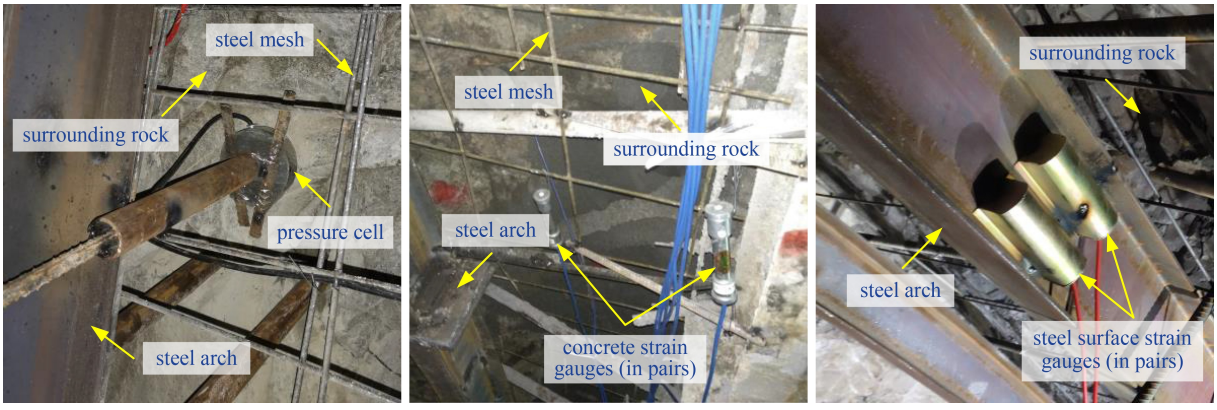

Fig. 10 Installation photo of the monitoring sensor.

convergence of the primary support. Monitoring data were collected manually using a data acquisition instrument every or every other day.

4.2 Monitoring results

Approximately 90 d after the installation of the sensors, the monitoring data were stable. At this time (denoted as t_0), the ST upper bench face was approximately −30 m away from the monitoring section. Therefore, the subsequent change in the monitoring data after t_0 can be considered to be induced only by ST construction. In this paper, the times at which the upper and lower benches of the ST were constructed to the monitoring section were recorded as t_1 and t_2, respectively, and time t_3 represents the time when the excavation of the ST upper bench pass a distance of 30 m through the monitoring section. The stress in shotcrete or steel arch can be calculated by multiplying the monitored strain using the corresponding elastic modulus. The internal force of shotcrete and steel arch can be calculated by Eq. (2).

4.2.1 Settlement and horizontal convergence

The evolution process of the settlement and horizontal convergence of the HRT primary support are plotted in Fig. 11. The *Y*-axis is the settlement or horizontal convergence value. The lower *X*-axis denotes the monitoring time. The upper *X*-axis represents the distance from the ST upper bench face to the monitoring section during construction. It is easy to find that both the settlement and horizontal convergence underwent a process of "slow change-rapid change-stable". Stage I: the settlement and horizontal convergence began to change when the ST upper bench face was −15.6 m (approximately 1.1*D*, *D* is the ST outer diameter) away from the monitoring section. The maximum deformation rate is 0.4 mm/d. Stage II: the deformation rate increased rapidly with the construction process and reached the maximum when the ST upper bench was excavated to the monitoring section. Stage III: the deformation rate decreased gradually, and the monitoring data tended to be stable when the excavation of the ST lower bench passed the monitoring section of 8.4 m (0.6*D*). Therefore, the longitudinal influence range of the ST construction on the HRT was approximately 0.6*D*–1.1*D*.

Within 6 d around the excavation of the ST upper bench passing the monitoring section, the deformation of the HRT primary support accounted for 33.3%–66.7% of the total deformation induced by ST construction, while the same situation for the ST lower bench accounted for only 5.3%–22.2%, which was far less than the former. This finding implies that the ST upper bench excavation mainly caused the HRT primary support deformation.

The initial ($t = t_0$) and final ($t = t_3$) settlement and horizontal convergence of the HRT primary support are

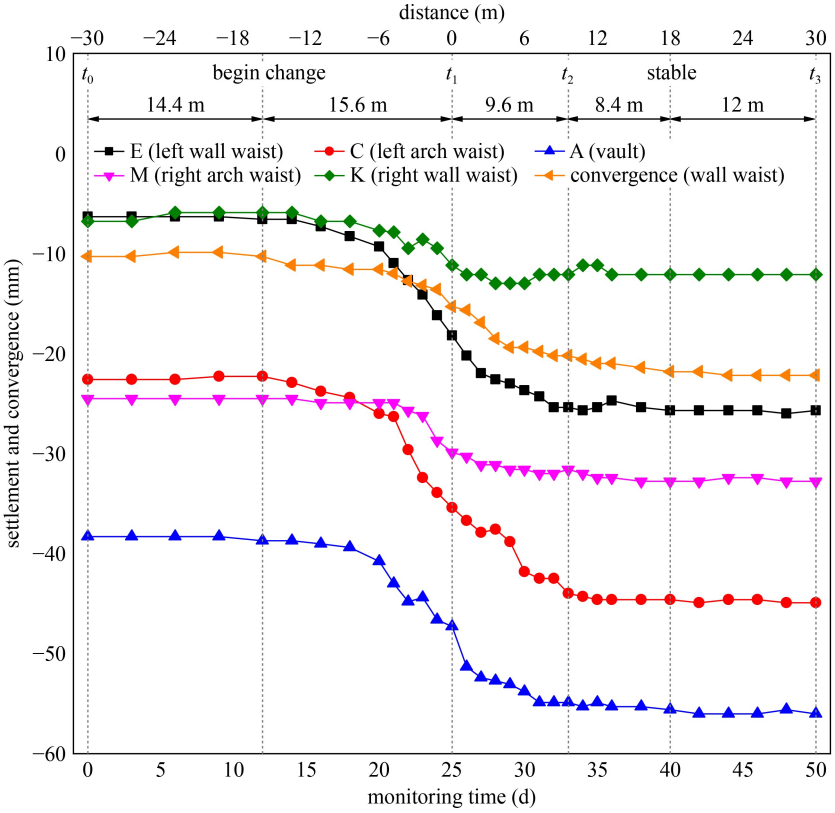

Fig. 11 Evolution process of the settlement and horizontal convergence of HRT primary support.

listed in Table 7. The settlement and horizontal convergence all increased under the disturbance of the ST construction. The horizontal convergence at the sidewall increased from −10.3 mm to −22.2 mm (an increase of 115.5%), indicating that the ST construction's influence on the HRT was very significant. The settlement at the left arch waist (C) changed the most, increasing from −22.6 to −44.9 mm. The least increase was at the right wall waist (K), which only increased by 5.3 mm. Overall, the primary support settlement on the left side (the side near the ST) of the HRT was significantly larger than that on the right side, showing that the ST construction influence on the left primary support of the HRT was greater than that on the right.

4.2.2 Surrounding rock pressure

The evolution process of the HRT surrounding rock pressure is shown in Fig. 12. The positive value denoted a compressive force between the surrounding rock and primary support. The surrounding rock pressure changed gradually since the ST upper bench face was −13.2 m (approximately 0.9*D*) away from the monitoring section and reached equilibrium after the excavation of the ST lower bench passed the monitoring section of 10.8 m (approximately 0.8*D*). This showed that the longitudinal influence range of the ST construction on the HRT was approximately 0.8*D*–0.9*D*. When the ST upper bench excavation reached the monitoring section, the pressure variation accounted for 24.2%–38.9% of the total variation induced by the ST construction, indicating that the rock pressure on the HRT changed dramatically before the ST upper bench was excavated as far as the monitoring section. This phenomenon could be attributed to the pre-settlement of the lagging ST [1,2].

The initial ($t = t_0$) and final ($t = t_3$) distributions of the HRT surrounding rock pressure are plotted in Fig. 13. The initial rock pressure was asymmetrically distributed

Table 7 The initial and final settlement and horizontal convergence of HRT primary support

type	settlement (mm)					convergence (mm)
	left wall waist (E)	left arch waist (C)	vault (A)	right arch waist (M)	right wall waist (K)	wall waist
initial ($t = t_0$)	−6.3	−22.6	−38.3	−24.5	−6.8	−10.3
final ($t = t_3$)	−25.7	−44.9	−56.0	−32.8	−12.1	−22.2
variation between t_0 and t_3	−19.4	−22.3	−17.7	−8.3	−5.3	−11.9

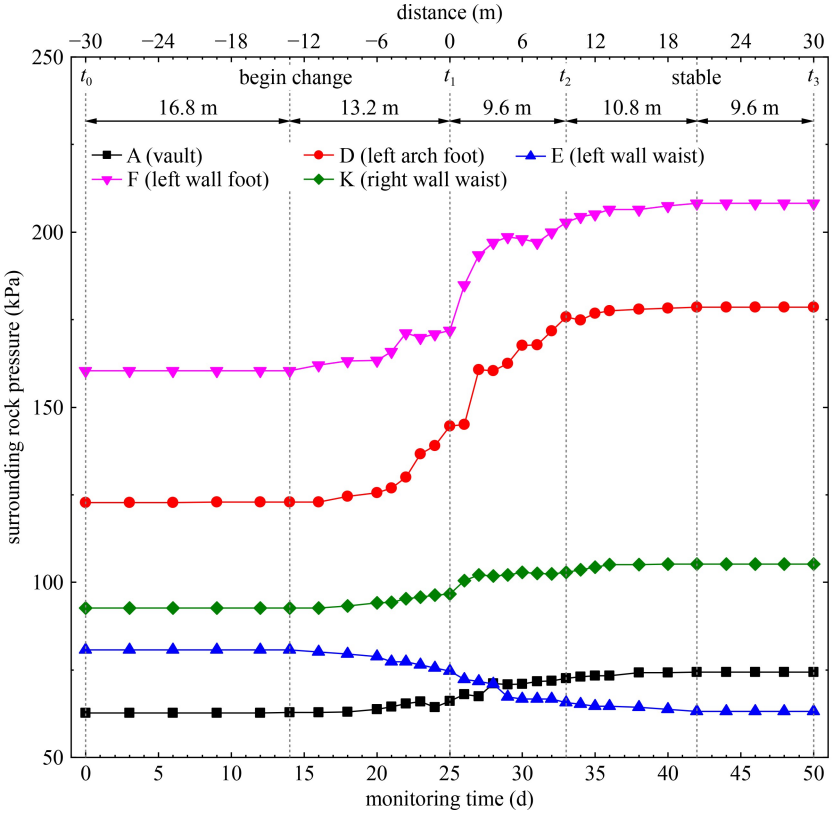

Fig. 12 Evolution process of the HRT surrounding rock pressure.

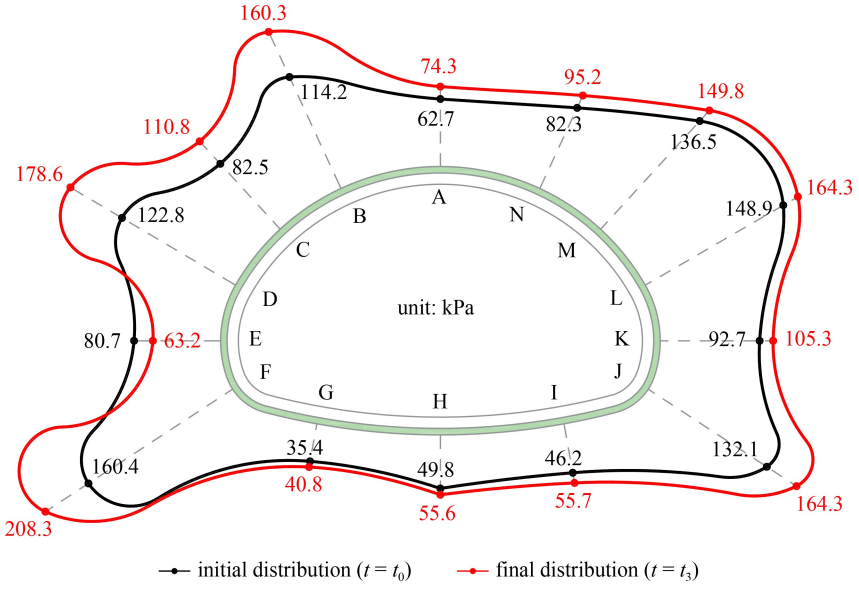

Fig. 13 The initial and final distribution of the HRT surrounding rock pressure.

along the centerline, and the highest rock pressure was 160.4 kPa, which was located at the left wall foot (F). The rock pressure at the invert (G, H, and I) was relatively small, and was no more than 50 kPa. The ST excavation heavily influenced the HRT pressure distribution. Except for the decrease at the left wall waist (E), the rock pressure at other parts of the HRT all increased. The maximum increase was 55.8 kPa, located at the left arch foot (D). It is easy to find that the pressure increases on the left side of the HRT (the side near the ST) were higher than those on the right by comparing the initial and final rock pressure distributions. This finding implied that the influence of the ST construction on the left surrounding rock of the HRT was greater than that on the right.

4.2.3 Internal force of the shotcrete

The evolution process of the circumferential stress in HRT shotcrete is shown in Fig. 14. The positive and negative values denoted compressive and tensile stresses, respectively. Note that the concrete strain gauges at the right arch shoulder (N) were damaged during construction, and no data were obtained. It is easy to find that the longitudinal influence range of the ST construction on the HRT was approximately 8.4 to 13.2 m (0.6D to 0.9D) according to the development trend of the circumferential stress. The stress variation during the excavation of the ST upper bench accounted for 62.5%–80.4% of the total variation induced by ST construction, while the same situation for the ST lower bench accounted for only 19.6%–37.5%. This phenomenon again demonstrated that the influence of the ST construction was mainly caused by ST upper bench construction.

The initial ($t = t_0$) and final ($t = t_3$) distributions of the circumferential stress and bending moment in HRT shotcrete are plotted in Fig. 15. The shotcrete was under compression, and the initial circumferential stress distribution was symmetrical. The circumferential stresses at the left and right wall waist (E and K) were relatively large, exceeding 10 MPa. The minimum circumferential stress was 0.03 MPa and was located at the middle invert (H). However, the circumferential stress of HRT shotcrete changed unevenly under the ST construction disturbance. The circumferential stress mainly increased, except for that at the vault (A), left arch shoulder (B) and left arch waist (C). The maximum increase was 2.48 MPa and was found at the left wall waist (E), and the minimum increase was only 0.07 MPa, located at the middle invert (H). As was the case for the deformation results, the stress increments on the left side of the HRT (the side near the ST) were larger than those on the right side, showing again that the influence of the ST construction on the left primary support of the HRT was more significant than that on the right.

The bending moment is an important physical quantity to characterize the mechanical state of concrete structures due to the low tensile strength of concrete [27]. At time t_0, the maximum positive bending moment of HTR shotcrete was 202.5 kN·m at the vault (A), whereas the minimum negative bending moment was –224.3 kN·m at the left arch shoulder (B). Under the disturbance of ST excavation, the bending moment in HRT shotcrete mainly increased except for that at the left arch waist (C) and left arch foot (D). The maximum increase was observed at the left invert (G), which increased from 46.3 to 122.7 kN·m. These findings indicate that the mechanical states of the vault, left arch waist and left invert were relatively unfavorable. To quantitatively evaluate HRT shotcrete safety, the minimum safety factors at times t_0 and t_3 are listed in Table 8. The minimum value was 1.61, which is

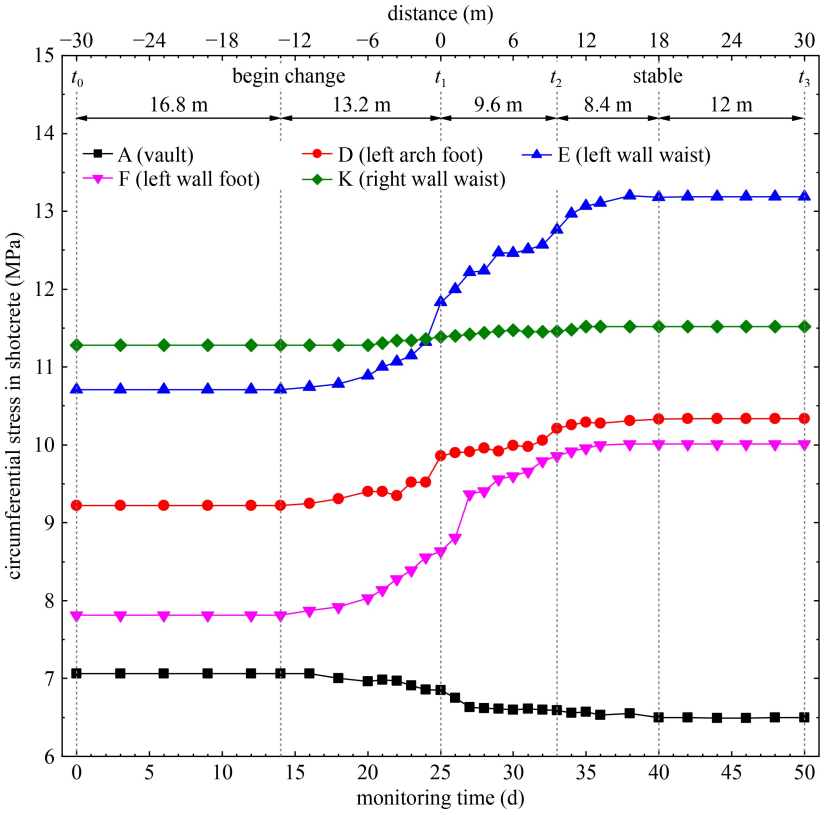

Fig. 14 Evolution process of the circumferential stress in HRT shotcrete.

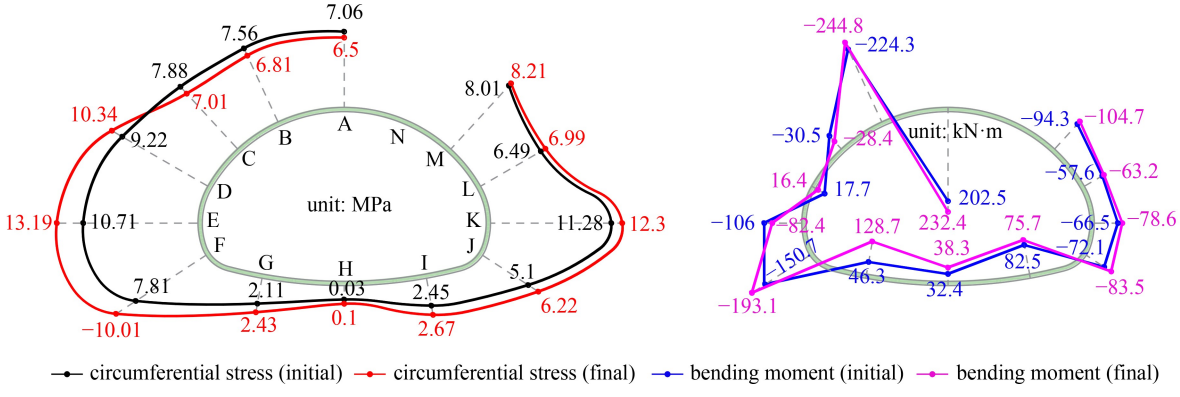

Fig. 15 Initial and final distribution of the circumferential stress and bending moment in HRT shotcrete.

Table 8 The minimum safety factors of HRT shotcrete at time t_0 and t_3

time	minimum safety factor (compressive strength control)		minimum safety factor (tensile strength control)	
	value	position	value	position
initial ($t = t_0$)	1.95	right wall waist (K)	3.25	middle invert (H)
final ($t = t_3$)	1.67	left wall waist (E)	1.61	left invert (G)

higher than 1.5 stipulated in the Code for Design of Railway Tunnel (TB10003-2016) [26], and no obvious crack was found in the shotcrete surface during the field construction. Therefore, it can be concluded that the HRT shotcrete was relatively safe.

4.2.4 Internal force of the steel arch

The evolution process of the axial stress in the HRT steel arch is shown in Fig. 16. The meanings of the positive and negative values were the same as those of circumferential stress in shotcrete. Note that the steel

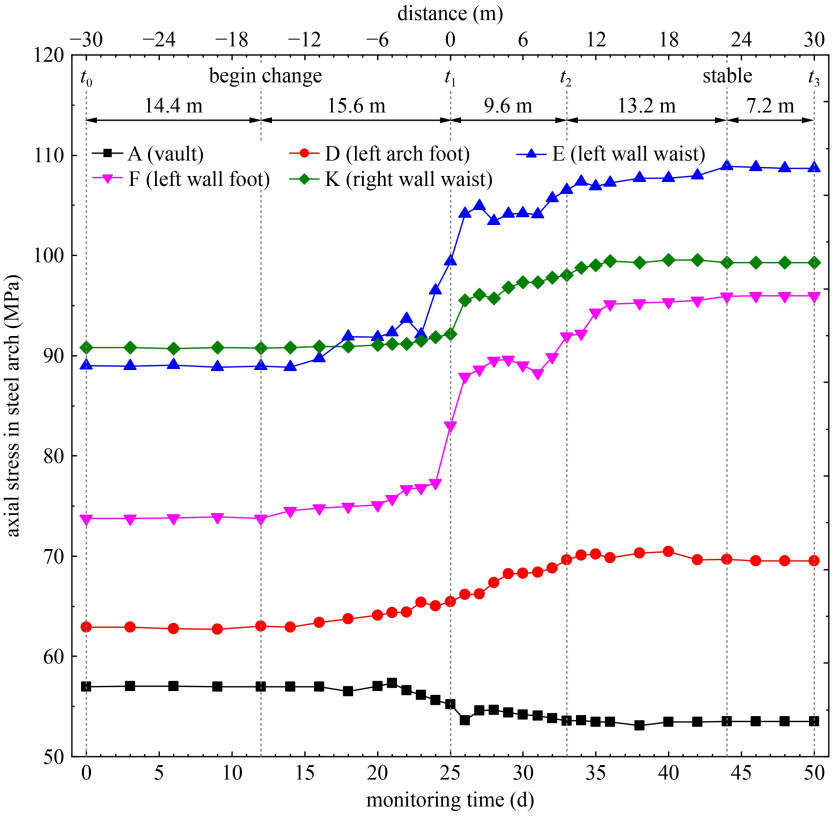

Fig. 16 Evolution process of the axial stress in HRT steel arch.

surface strain gauges at the middle and right invert (H and I) were damaged during construction. The longitudinal influence range of the ST construction on the HRT was approximately 13.2–15.6 m (0.9*D*–1.1*D*) from the development trend of the axial stress. The stress variations induced by ST upper bench excavation accounted for 70.6%–79.9% of the total variations, whereas the variations caused by ST lower bench excavation accounted for only 20.1%–29.4%. The direction and development of the axial stress in HRT steel arch was in good agreement with the circumferential stress in HRT shotcrete, differing only in magnitude. This finding implied that the shotcrete and steel arch bear the load together and showed compatible deformation behavior.

The initial ($t = t_0$) and final ($t = t_3$) distributions of the axial stress and bending moment in the HRT steel arch are plotted in Fig. 17. The HRT steel arch mainly endured compressive stress, and the initial axial stress distribution was symmetrical. The maximum value was 90.8 MPa, located at the right wall waist (K). The minimum value was 22.45 MPa, located at the left invert (G). The axial stress of the HRT steel arch changed greatly under the ST excavation disturbance, particularly on the left side (the side near the ST). The stress increment was 19.67 MPa at the left wall waist (E) and 22.22 MPa at the left wall foot (F). However, the stress increase on the right side was relatively smaller, which was only 8.47 MPa at the right wall waist (K) and 3.68 MPa at the right wall foot (J).

Compared with that of the HRT shotcrete, the bending moment of the HRT steel arch was lower. At time t_0, the maximum positive bending moment of the HRT steel arch was 10.21 kN·m at the vault (A), while the minimum negative bending moment was –12.33 kN·m at the left arch shoulder (B). Although the bending moment mainly increased under the disturbance of the ST excavation, there was little effect on the safety of the steel arch in general since the steel arch has high tensile strength. The safety of the steel arch was directly evaluated by comparing the monitoring data with the steel strength (which is 205 MPa for Q235 steel). The minimum safety factor in the whole construction process was 1.89, which was much larger than 1.0, indicating that the HRT steel arch was safe.

The axial force is an intuitive parameter to characterize the mechanical state of the structure, which can be calculated by multiplying the stress by the cross-sectional area. Within the unit grid spacing (0.8 m), the cross-sectional areas of HRT shotcrete and steel arch were 0.4 m^2 and 39.578 cm^2, respectively. The final axial forces in the HRT shotcrete and steel arch were calculated and are listed in Table 9. The final axial force distributions of the shotcrete and steel arch were relatively similar. This phenomenon could be explained by that the steel arch and shotcrete bore load mutually and deformed compatibly during construction. The final axial force in the shotcrete was approximately 9–16 times

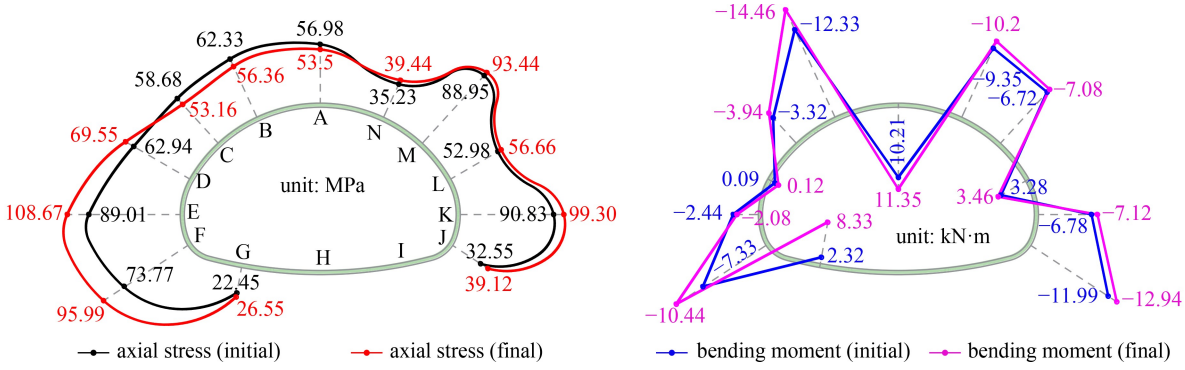

Fig. 17 Initial and final distribution of the axial stress and bending moment in HRT steel arch.

Table 9 The final axial force in shotcrete and steel arch

position	shotcrete ($\times 10^3$ kN)	steel arch ($\times 10^3$ kN)	shotcrete/steel arch
A	2.60	0.212	12.3
B	2.72	0.223	12.2
C	2.80	0.210	13.3
D	4.14	0.275	15.0
E	5.28	0.430	12.3
F	4.00	0.380	10.5
G	0.97	0.105	9.2
H	0.04	–	–
I	1.07	–	–
J	2.49	0.155	16.1
K	4.92	0.393	12.5
L	2.80	0.224	12.5
M	3.28	0.370	8.9
N	–	0.156	–

that of the steel arch at the same position. In the HRT primary support, the cross-sectional area of the shotcrete was approximately 101 times that of the steel grid, while the elastic modulus of the steel arch was approximately 7 times that of the shotcrete. Therefore, the axial force of the shotcrete should theoretically be approximately 14.4 times that of the steel arch, which was relatively consistent with the monitoring results. This finding implied that the monitoring results were relatively reasonable, and the shotcrete was the main bearing structure of the HRT primary support.

4.2.5 Comparison of simulation results and monitoring data

To verify the numerical model accuracy and excavation method rationality, the HRT vault settlement, wall waist convergence and lining stress in numerical simulation and field monitoring were comprehensively compared. As shown in Fig. 18, the developments of the vault settlement and wall waist convergence in numerical simulation were close to that in field monitoring. The maximum values of the calculated and measured vault settlement were − 59.3 and − 56 mm, respectively, the relative error was within 10%. For the wall waist convergence, the maximum difference between numerical simulation and field monitoring was only 3.0 mm. As displayed in Fig. 19, the simulated and monitored final stress distributions of HRT lining were relatively similar. The lining stresses at the tunnel side wall were commonly larger than 10 MPa, while the stresses at the tunnel arch and invert were relatively small. The average of the lining stress in numerical simulation (7.51 MPa) was close to that in field monitoring (7.14 MPa), the relative error was approximately 5%. These phenomena showed that the simulation results were consistent with the monitoring data. Therefore, the numerical model was accurate, and the excavation method was feasible.

5 Parametric studies

The relative position, excavation method and excavation footage of the double tunnels significantly affected the tunnel response [6]. As shown in Fig. 20, the relative position of the double tunnels could be characterized by the relative angle β and pillar width L. β was defined as positive when ST was located above HRT. Based on numerical simulation, the effects of relative angle β, pillar width L, ST excavation method and excavation footage S on HRT response were studied comprehensively. The calculation parameters of the surrounding rock and supporting structure were consistent with the values in Subsection 3.2.

The effect of β is shown in Fig. 21(a). When β was −45°, the lining stress of HRT at the left wall waist increased by 25.6% due to the ST construction, which can seriously threaten the safety of HRT. On the contrary, ST construction had little effect on HRT when β was 45°; the stress increases were within 5%. Therefore, for double tunnels located at different levels, the tunnel below should be excavated first to reduce the influence of lagging tunnelling on leading tunnel. HRT and ST were

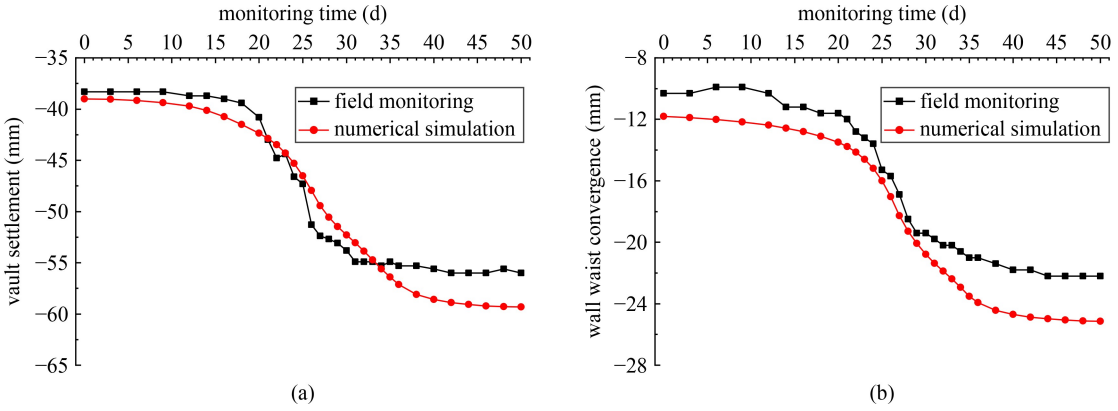

Fig. 18 Comparison between the calculated and measured lining deformations. (a) Vault settlement; (b) wall waist convergence.

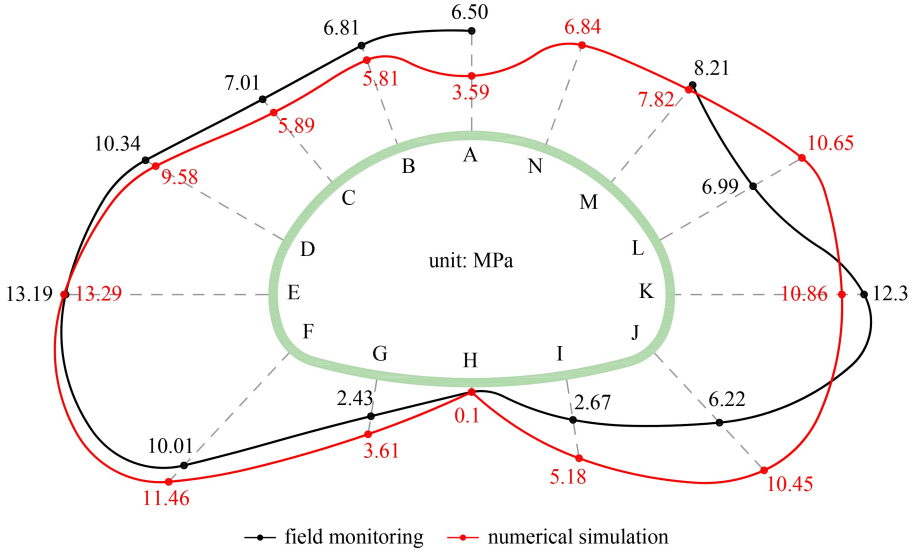

Fig. 19 Comparison between the calculated and measured lining stresses.

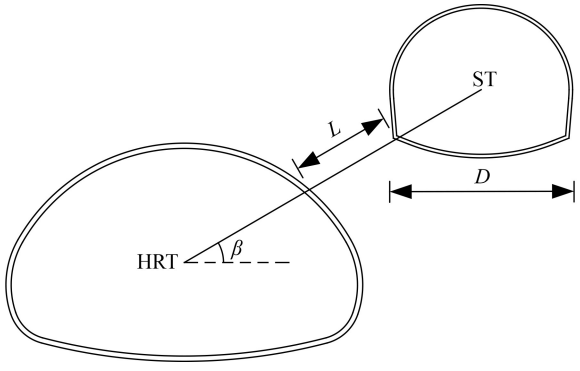

Fig. 20 Relative position of double tunnels.

horizontally aligned when β was 0°, and vertically was aligned when β was −90° or 90°, which are the common arrangements in double tunnels. However, the ST excavation significantly affected the HRT lining stress (increases by 10%–20%) under these common arrangements.

The effect of L is displayed in Fig. 21(b). With the decrease of L, the ST excavation disturbance on HRT became extremely significant. When L was 0.5 D (D is the ST outer diameter), the lining stress of HRT at the wall waist increased by 41.9%, which was extremely unfavorable. The stress variations were within 10% when L was larger than 2.0D, indicating that the influence of the lagging tunnelling on the leading tunnel can be well controlled when L was larger than 2 times the outer diameter of the lagging tunnel. When L was greater than 4.0D, the lining stress of HRT was almost constant, implying that the ST construction disturbance on HRT basically disappeared.

Figure 21(c) displays the effect of ST excavation method, M1–M5 in the figure represent full face method, common bench cut method (without a temporary inverted arch), bench cut method with a temporary inverted arch, CD method and CRD method, respectively. The ST excavation method significantly affected the HRT lining stress. When full face method was adopted, the lining stress of HRT at the wall waist increased by 20.2%, while the stress increase was within 10% when CD method or

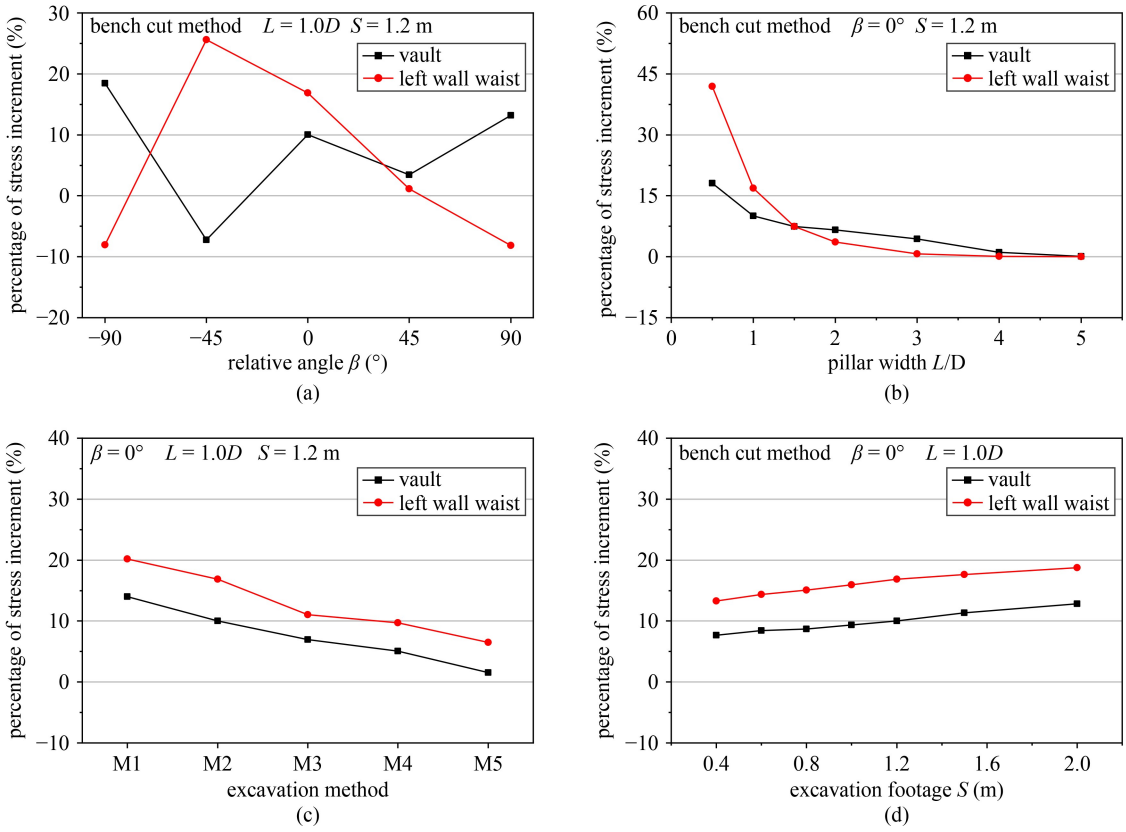

Fig. 21 Effect of relative angle, pillar width, ST excavation method and excavation footage on HRT response. (a) Relative angle; (b) pillar width; (c) ST excavation method; (d) excavation footage.

CRD method was used. For bench cut method, the maximum stress variation of HRT lining was significantly reduced (from 16.9% to 11.1%) when a temporary inverted arch was applied.

The effect of S is shown in Fig. 21(d). With the decrease of S, the ST excavation disturbance on HRT reduced gradually. When S was 2.0 m, the maximum stress increase in HRT lining was 18.8%, located at the left wall waist. When S decreased to 0.4 m, the maximum stress increase of HRT lining decreased to 13.3%.

6 Design and construction optimization

Although the simulation results and monitoring data of the HRT lining showed that the "yielding principle" design could meet the structural safety requirements, the structural stability should also be taken into consideration. According to the monitoring data and parameter analysis results, the following suggestions are proposed.

The development and distribution characteristics of the HRT lining deformation, surrounding rock pressure and lining internal force indicate that the ST construction influence on the left lining (the side near the ST) of HRT is much larger than that on the right side. The lining stresses of HRT at left arch foot, left wall waist and left wall foot increase by 15%–30% due to the ST excavation disturbance, which is extremely unfavorable to the safety of HRT. Therefore, the left lining of HRT, especially in the left arch foot, left wall waist and left wall foot areas, should be strengthened. Appropriately improving the strength grade of the shotcrete and steel arch, increasing the lining thickness of the sidewall, using larger diameter footing-reinforcement pipes, or increasing the distribution density or the length of the systematic bolts are effective methods to improve the bearing capacity of the HRT left lining [28].

Effective measures to control the ST excavation disturbance are also required. The monitoring data show that the ST excavation disturbance is mainly generated in the excavation of the upper bench. This phenomenon could be explained by that the ST lining cannot form a closed ring after the upper bench excavation. Compare with the common bench cut method (without a temporary inverted arch), the ST excavation disturbance on HRT is significantly reduced (approximately 30%) when a temporary inverted arch is applied. Moreover, the excavation footage also affects the ST construction disturbance. Therefore, to reduce the stress variation of HRT lining during the ST construction, a temporary inverted arch or CD/CRD method should be adopted in ST excavation. Additionally, the ST excavation footage should be reduced.

The rock quality has a significant influence on the

interaction of double tunnels since the excavation disturbance of lagging tunnel affects the mechanical behavior of leading tunnel through the pillar [13,29]. Thus, the pillar quality should be strengthened to weaken the ST excavation disturbance on HRT. For example, deep hole grouting reinforcement and long pre-tensioned bolts with large support density can be adopted.

7 Conclusions

Based on the closely spaced tunneling of a super-span HRT and a large-span ST in strongly weathered tuff strata, the structural design of the HRT considering the ST construction disturbance was analyzed using numerical simulation. The mechanical response of HRT during ST construction was comprehensively investigated using field monitoring. The main conclusions are summarized below.

1) The rational structural design of HRT considering the ST construction disturbance was determined based on the simulation results. The "yielding principle" design and the "resistance principle" design were feasible given the safety of HRT linings, and there was little difference between the two designs in the vertical displacement and plastic zone of the surrounding rock. However, the minimum safety factor of the HRT secondary lining in the "yielding principle" design was approximately 2 times that in the "resistance principle" design. Therefore, the "yielding principle" design was adopted considering the safety and durability of the HRT secondary lining.

2) The disturbance characteristics of the ST construction on the HRT were analyzed and summarized according to the monitoring data. The longitudinal influence range of the ST construction on the HRT was approximately $0.6D$–$1.1D$ (where D is the ST outer diameter). Under the ST construction disturbance, the increments of the lining deformation, surrounding rock pressure and lining internal force on the left side (the side near the ST) of the HRT were much greater than those on the right side. The stress increase of the HRT primary support during the ST upper bench excavation accounted for 62.5%–80.4% of the total increment, showing that the ST construction disturbance was mainly generated in the ST upper bench excavation.

3) The safety status of the HRT primary support was assessed according to the internal force of the shotcrete and steel arch. The HRT shotcrete and steel arch mainly endured compressive stress during ST construction. The minimum safety factors of the HRT shotcrete and steel arch were 1.61 and 1.89, respectively, which were larger than the specified value of 1.5, indicating that the HRT primary support was in an appropriate and safe working state.

4) The HRT steel arch and shotcrete bore load mutually and displayed compatible deformation behavior. According to the monitoring data, the evolution process and distribution characteristics of the internal force in the shotcrete and steel arch were relatively similar. The final axial force in shotcrete was approximately 9–16 times that of the steel arch at the same position, which was in good agreement with the theoretical results. The shotcrete was the main bearing support structure of the HRT primary support.

5) Parametric studies were performed to investigate the effects of relative angle, pillar width, ST excavation method and excavation footage on HRT response. Results showed that the most critical parameters were the relative angle and pillar width, which determined the relative position of HRT and ST, followed by the ST excavation method, which showed that the rapid closure of ST lining can effectively reduce the ST excavation disturbance, and the excavation footage.

6) According to the monitored data and parameter analysis results, some engineering suggestions, such as improving the bearing capacity of the HRT left lining, optimizing the ST excavation method and excavation footage, and strengthening the pillar quality, were proposed for closed spaced super-span tunnels.

Acknowledgements The authors gratefully acknowledge the support provided by the China Railway Bridge Bureau Group (No. CL19048530); the China Railway Design Group (No. 721602). In addition, the authors thank American Journal Experts (AJE) for its linguistic assistance during the preparation of this manuscript. No conflict of interest exists in the submission of the manuscript.

References

1. Li R, Zhang D L, Fang Q, Liu D P, Luo J W, Fang H C. Mechanical responses of closely spaced large span triple tunnels. Tunnelling and Underground Space Technology, 2020, 105: 103574
2. Luo J W, Zhang D L, Fang Q, Liu D P, Xu T. Mechanical responses of surrounding rock mass and tunnel linings in large-span triple-arch tunnel. Tunnelling and Underground Space Technology, 2021, 113: 103971
3. Wu L, Zhang X D, Zhang Z H, Sun W C. 3D discrete element method modelling of tunnel construction impact on an adjacent tunnel. KSCE Journal of Civil Engineering, 2020, 24(2): 657−669
4. Do N A, Dias D, Oreste P, Djeran Maigre I. Three-dimensional numerical simulation of a mechanized twin tunnels in soft ground. Tunnelling and Underground Space Technology, 2014, 42: 40−51
5. Tu H L, Zhou H, Qiao C S, Gao Y. Excavation and kinematic analysis of a shallow large-span tunnel in an up-soft/low-hard rock stratum. Tunnelling and Underground Space Technology, 2020, 97: 103245
6. Hage Chehade F, Shahrour I. Numerical analysis of the interaction between twin-tunnels: Influence of the relative position and construction procedure. Tunnelling and Underground Space

Technology, 2008, 23: 210−214
7. Chen S L, Lee S C, Gui M W. Effects of rock pillar width on the excavation behavior of parallel tunnels. Tunnelling and Underground Space Technology, 2009, 24: 148−154
8. Das R, Singh P K, Kainthola A, Panthee S, Singh T N. Numerical analysis of surface subsidence in asymmetric parallel highway tunnels. Journal of Rock Mechanics and Geotechnical Engineering, 2017, 9: 170−179
9. Banerjee S K, Chakraborty D. Behavior of twin Tunnels under different physical conditions. International Journal of Geomechanics, 2018, 18(8): 06018018
10. Sahoo J P, Kumar J. Stability of long unsupported twin circular tunnels in soils. Tunnelling and Underground Space Technology, 2013, 38: 326−335
11. Boon C W, Ooi L H. Longitudinal and transverse interactions between stacked parallel tunnels constructed using shield tunnelling in residual soil. Geotechnical Engineering Journal of the SEAGS & AGSSEA, 2018, 49(2): 57−71
12. Li P, Wang F, Fan L, Wang H, Ma G. Analytical scrutiny of loosening pressure on deep twin-tunnels in rock formations. Tunnelling and Underground Space Technology, 2019, 83: 373−380
13. Choi J, Lee S. Influence of existing tunnel on mechanical behavior of new tunnel. KSCE Journal of Civil Engineering, 2010, 14(5): 773−783
14. Boonyarak T, Ng C W W. Effects of construction sequence and cover depth on crossing-tunnel interaction. Canadian Geotechnical Journal, 2015, 52(7): 851−867
15. Cooper M L, Chapman D N, Rogers C D F, Chan A H C. Movements in the Piccadilly Line tunnels due to the Heathrow Express construction. Geotechnique, 2002, 52(4): 243−257
16. Wang Z, Yao W, Cai Y, Xu B, Fu Y, Wei G. Analysis of ground surface settlement induced by the construction of a large-diameter shallow-buried twin-tunnel in soft ground. Tunnelling and Underground Space Technology, 2019, 83: 520−532
17. Golshani A, Varnusfaderani M G. Innovative design modification during construction of a twin tunnel using real-time field data. Transportation Geotechnics, 2019, 20: 100254
18. Huang Z, Zhang C, Fu H, Deng H, Ma S, Fu J. Numerical study on the disturbance effect of short-distance parallel shield tunnelling undercrossing existing tunnels. Advances in Civil Engineering, 2020, 2020(2): 1−14
19. Zhang D L, Fang Q, Hou Y, Li P, Yuen Wong L N. Protection of buildings against damages as a result of adjacent large-span tunneling in shallowly buried soft ground. Journal of Geotechnical and Geoenvironmental Engineering, 2013, 139(6): 903−913
20. Cantieni L, Anagnostou G. The interaction between yielding supports and squeezing ground. Tunnelling and Underground Space Technology, 2009, 24: 309−322
21. Zhou J, Yang X A, Cai J, Yang F. Distribution rules of loads on composite lining in deep-buried tunnels and mechanical solutions of loads. Chinese Journal of Rock Mechanics and Engineering, 2021, 40(5): 1009−1020 (in Chinese)
22. Song C Y, Tu H L, Qiao C S. Analysis on combination mode and parameters of primary support of shallow-buried large-span tunnel: Case study on Xinggongjie station tunnel on No. 2 line of Dalian metro. Tunnel Construction, 2015, 35(6): 491−499 (in Chinese)
23. Marinos P, Hoek E. GSI: A geologically friendly tool for rock mass strength estimation. In: GeoEng 2000. Melbourne: Taylor & Francis, 2000
24. Hoek E, Brown E T. The Hoek–Brown failure criterion and GSI—2018 edition. Journal of Rock Mechanics and Geotechnical Engineering, 2019, 11: 445−463
25. Zhang H J, Qiu W G, Qing W C. Study on distribution of axial forces of systematic anchor bars in tunnel multi-partition excavation. Journal of the China Railway Society, 2013, 35(12): 90−94 (in Chinese)
26. TB10003-2016. Code for Design on Railway Tunnel. Beijing: China Railway Publishing House Co., Ltd., 2016 (in Chinese)
27. Hibbeler R C. Statics and Mechanics of Materials. Upper Saddle River: Prentice Hall, 2014
28. Luo J, Zhang D, Fang Q, Li A, Sun Z, Cao L. Analytical study on pretensioned bolt-cable combined support of large cross-section tunnel. Science China. Technological Sciences, 2020, 63(9): 1808−1823
29. Sterpi D, Cividini A. A Physical and numerical investigation on the stability of shallow tunnels in strain softening media. Rock Mechanics and Rock Engineering, 2004, 37(4): 277−298